COVER SHEET

MID-INFRARED AND INFRARED EMISSION SPECTROSCOPY OF Cu-EXCHANGED MONTMORILLONITE

J. Theo Kloprogge*, Emir Mahmutagic and Ray L. Frost
Inorganic Materials Research Program, School of Physical and Chemical Sciences, Queensland University of Technology, GPO Box 2434, Brisbane, Q 4001, Australia

* Corresponding author
Phone: +61 7 3864 2184, fax +61 7 3864 1804, E-mail t.kloprogge@qut.edu.au

ABSTRACT
Middle Infrared Spectroscopy (Mid-IR) and Infrared Emission Spectroscopy (IES) were employed to characterise Cu-exchanged montmorillonites, which were derived from two different types of montmorillonite clays, Ca-exchanged montmorillonite (Cheto clay) and Na-exchanged montmorillonite (Miles clay). Copper was exchanged under both acidic and basic conditions at different Cu / clay ratios. All Cu-exchanged montmorillonites experienced a shift in most of non-lattice bands, with hydroxyl bands playing a major role in the characterisation of the clays. Furthermore, a relationship between the ratio of bands at 3630 and 3500 cm^{-1} and the Cu-concentration of the starting solutions was indicated and used to compare the degree of cation exchange between two preparation methods. Two dehydration stages were observed in the IES experiments. Additional bands were observed in all Cu-exchanged montmorillonites prepared with the 'basic conditions method', and these bands were assigned to ammonia molecules trapped within the clay structure or absorbed on the surface of the clay.

Key words: copper exchange; infrared spectroscopy; infrared emission spectroscopy; montmorillonite; wet oxidation

INTRODUCTION

Clay minerals are some of the most versatile and therefore most studied type of minerals. Their importance is further highlighted with their abundance, as they comprise as much as 40% of the minerals in sedimentary rocks [1].

Montmorillonite was the name given to a clay mineral found near Montmorillon in France as long ago as 1874 [2]. It is classified as a dioctahedral clay with the 2:1 layer linkage, and belongs to a highly disordered group of smectites [3]. Water molecules are readily absorbed by montmorillonite, forming hydration shells around the interlayer cations rather than continuous sheets [4]. Cation exchange capacity (CEC) is defined as the maximum amount of any one cation that can be taken up by a given clay [3]. This value is constant and clay specific. Montmorillonite, and what is typical for smectites in general, has a high cation exchange capacity, which ranges from 70 to 130 meq per 100g. Most of the exchange capacity (80%) is due to substitution within the structure, but a lesser amount (20%) is due to the charges at the edge of the sheets [1].

Aluminosilicates as catalyst materials were developed at the same time as the concept of heterogeneous catalysis was created. Considering their abundance, clay minerals were the obvious choice for the investigation of their catalytical activity [5]. The use of clays as cracking catalysts for gasoline production was investigated in the first half of the 20th century, but catalytic cracking did not become commercially feasible until the catalyst regeneration process was developed [6].

Today, clay catalysts still remain as a significant contender, although in a significantly different structural form. While zeolites are multicomponent catalysts with the aluminosilicate matrix, pillared clays are practically an expanded form of smectites formed by an introduction of a large interlayer cation [7, 8]. Many researchers, however, are going back to basics by working with traditional clays to get a better understanding of the catalytic mechanism and substance selectivity [9-11].

The use of copper is of particular importance, because of its catalytic performance in the reactions such as wet air oxidation, photocatalytic oxidation for wastewater treatment and selective catalytic reduction of NO [11, 12]. On the other hand, montmorillonite possesses several interesting characteristics, such as swellability and exchangeability, which make it an attractive support material. Once acid activated, montmorillonite acquires a catalytic activity index of 40 and a fairly large surface area of around 300 m^2g^{-1} [12]. An example of the high selectivity of Cu-exchanged montmorillonite is the conversion of methanol into only one product, DME, which is not the case with some other catalysts including Cu-exchanged laponite and Cu-exchanged saponite where more than one product is formed [11].

Another significant application is of great interest in environmental and soil science [9]. In this respect, clay minerals may fix metals through ion exchange [13, 14] or surface complexation [15]. Clay minerals would be a great choice for use as geochemical barriers against diffuse aquatic pollutions such as observed in:

- suspended matters from wastewaters and polluted rivers [16]
- soils near smelter complexes [17]
- sediments from settling basins , near motorways [18].

Furthermore, ion exchanging clay minerals could find their way into low-cost cleaning systems for industrial effluents and wastewaters [19, 20].

There are two simultaneous events, which lead to the collapse of the structure of Cu-exchanged montmorillonite at elevated temperature, one being clay dehydration and the other copper migration. While still doubtful, a theory has been developed that the dehydration of montmorillonite occurs in two or more definite stages. The first stage is considered to be the loss of moisture from the clay surface with temperatures up to 150°C. This is then followed with the evolving of the water that is part of the structure, as the hydration shell of a cation,

in the temperature range 150-300°C. A third stage, only sometimes observed, arises from some cations possessing more than one hydration shell layer [2, 3, 21].

Copper cation migration mechanism theory is also a debatable subject but still provides some insight into possible solutions that can explain experimental observations. Many authors agree that for temperatures up to 200°C, Cu migrates into hexagonal cavities[14]. Above 200°C Cu will start penetrating into the octahedral sheets, where they saturate the charge of the sheet [22-24]. Once the Cu cations enter the octahedral sheets, they become "fixed" or non-exchangeable. The CEC is significantly reduced and is mainly due to charged sites on the edge of the montmorillonite sheets or to the small number of possible tetrahedral substitutions. Above 800°C major structural changes occur in montmorillonite. For example, cristobalite and mullite develop at about 1000 and 1100°C, respectively in the Wyoming-type clay [12, 21].

This paper describes the effect of copper exchange on two types of montmorillonite. Infrared emission spectroscopy is combined with mid-infrared spectroscopy in order to gain a better understanding of the behaviour of copper in the interlayer of the clay. Infrared emission spectroscopy allows one to study to the thermal behaviour of the copper-exchanged montmorillonite in-situ.

EXPERIMENTAL

Material preparation

Copper-exchanged montmorillonite samples were prepared from two types of montmorillonite. They were Cheto montmorillonite (Ch) from Clay Minerals Repository, University of Missouri-Columbia, and Miles montmorrillonite (Mi) received from Integrated Mineral Technology, Australia[25]. Cheto montmorillonite is mainly Ca-exchanged, while Miles monmorillonite is mainly Na-exchanged. Both clays were used as received without size separation and Na-exchange. The CEC of the Miles montmorillonite is about twice that of the Cheto montmorillonite

For copper loading, two exchange conditions were used. The first group was exchanged under acidic conditions where $Cu(NO_3)_2 \cdot 2.5H_2O$ solution was directly used for cation exchanging and this method is referred to as Series a. Under the second condition, ammonia was mixed with $Cu(NO_3)_2 \cdot 2.5H_2O$ and this basic solution (pH = 12) was then added to the clay suspension and this method is referred to as Series b. In each case, three different concentrations of copper solutions were added to the clay suspension, which resulted in 12 samples all together. All samples were washed with de-ionised water and dried at 80°C.

Analytical techniques

Mid-infrared spectra were obtained on a Perkin Elmer 1600 Fourier transform infrared spectrometer equipped with a DTGS detector. For each sample, 64 scans were recorded in the 4000-400 cm^{-1} spectral range in the absorbance mode with a resolution of 4 cm^{-1}. Spectra were recorded at room temperature using the KBr pressed disc technique (0.8 mg of sample and 270 mg of KBr).

FTIR emission spectroscopy was carried out on a Nicolet Fourier transform infrared spectrometer equipped with a MCT/A detector, which was modified by replacing the IR source with an emission cell. A description of the cell and principles of the emission experiment have been published elsewhere structures [26-28] . Approximately 0.2 mg of the clay sample was spread as a thin layer on a 6 mm diameter platinum surface and held in an inert atmosphere within a nitrogen-purged cell during heating. The infrared emission cell consists of a modified atomic absorption graphite rod furnace, which is driven by a thyristor-

controlled AC power supply capable of delivering up to 150 amps at 12 volts. A platinum disk acts as a hot plate to heat the sample and is placed on the graphite rod. An insulated 125-μm type R thermocouple was embedded inside the platinum plate in such a way that the thermocouple junction was <0.2 mm below the surface of the platinum. Temperature control of ± 2°C at the operating temperature of the saponite sample was achieved by using a Eurotherm Model 808 proportional temperature controller, coupled to the thermocouple. The emission spectra were collected at intervals of 50°C over the range 200 - 750 °C. The time between scans (while the temperature was raised to the next hold point) was ± 100 seconds. It was considered that this was sufficient time for the heating block and the powdered sample to reach temperature equilibrium. The spectra were acquired by co-addition of 64 scans for the whole temperature range (approximate scanning time 45 seconds), with a nominal resolution of 4 cm^{-1}. Good quality spectra can be obtained provided the sample thickness is not too large. If too large a sample is used then the spectra become difficult to interpret because of self-absorption. Spectral manipulation such as baseline adjustment, smoothing and normalisation was performed using the Spectracalc software package (Galactic Industries Corporation, NH, USA).

RESULTS AND DISCUSSION

Mid-infrared analysis

Cheto vs Miles OH-stretching region

In the range characteristic to OH stretching vibrations (Table 1, Fig. 1a), both samples have a medium absorption band around 3630 cm^{-1} (Cheto) and 3635 cm^{-1} (Miles), associated with the OH-group coordinated to two Al cations [24]. A very broad absorption in the range 3600-3000 cm^{-1} in fact consists of at least three different bands in both montmorillonites. OH-groups involved in H_2O-H_2O H-bonds absorb around 3470 and 3400 cm^{-1} (Cheto) and 3480 and 3400 cm^{-1} (Miles), while the shoulder between 3200 and 3400 cm^{-1} is ascribed to an overtone of the H_2O bending vibration. Absorptions below 3200 cm^{-1} is enhanced by the presence of small, strongly polarising cations, such as Al^{3+}, since H_2O molecules coordinated to them form stronger H-bonds to H_2O in outer spheres of coordination [29].

The major difference in this region appears to be the presence of organic compounds in Cheto montmorillonite. While small peaks around 2850 and 2925 cm^{-1}, visible in both spectra, are due to a thin polymeric film on the surface of the DTGS detector, extra bands are observed for the Cheto clay, which disappear after washing.

Cheto vs Miles low wavenumber region

The most intense bands due to the Si-O-Si stretching mode are observed around 1090 and 1040 cm^{-1} in Cheto montmorillonite (Fig. 1b) and for Miles montmorillonite at 1100 and 1050 cm^{-1}, respectively. The (Al_2OH) and (MgAlOH) deformation bands are found for the Cheto clay around 910 and 840 $cm^{-1}$and at a slightly higher wavenumbers for the Miles clay. The Si-O bending vibrations at 520 cm^{-1}, due to Si-O-Al, and at 467 cm^{-1}, due to Si-O-Si, are the same for both clays. This is also true for the H_2O -bending mode at approximately 1635 cm^{-1}, which in both spectra it consists of more than one band, which is probably due to a difference in coordination within the structure and the hydration shell. The most significant difference between the two samples is the presence of quartz in the Miles clay with bands around 800 and 780 cm^{-1}.

Cu-exchanged Cheto montmorillonite

There are only minor changes in the lower frequency range (1800-400 cm^{-1}) of Series a Cu-exchanged Cheto montmorillonites when compared to the spectrum of the starting clay (Fig. 2). In

the Cu-exchanged montmorillonites, the H_2O bending vibration at 1691 cm^{-1} is shifted slightly to a lower wavenumber, 1680 cm^{-1}, probably due to the change in the clay composition. Organic compounds from the starting Cheto montmorillonite, in the 1500-1300 cm^{-1} and also 3000-2800 cm^{-1} regions, appear to be mostly eliminated through the washing procedure. Instead, a new band emerges around 1400 cm^{-1} due to ammonia molecules being trapped in the structure.

The Al_2OH stretching mode at 3630 cm^{-1}, remains unchanged with the Cu loading. All other OH-group bands are shifted slightly downwards, about 5 to 20 cm^{-1} in the incremental steps depending on the starting Cu solution concentration, while the (cation-OH) H-bond is shifted upwards in a similar fashion. What appears to be important is the ratio of the bands at 3630 and 3470-3490 cm^{-1}, as different Cu loadings are applied. As more Cu is exchanged with Ca in Cheto montmorillonite, the hydration peak intensity decreases consistent with the fact that Ca coordinates higher amounts of H_2O than Cu (Fig. 3a) [29, 30]. When the ratio of the intensities of the (cation-OH) H-bonded band over (Al_2OH) stretching band is plotted against the Cu concentration of the starting solution, a reasonably good polynomial trendline can be fitted to the obtained curve, following, more or less, a linear trend until it reaches the concentration used for Cha1 sample after which it flattens out.

There appears to be even smaller changes in the infrared spectra of Series b Cu-exchanged Cheto montmorillonites when compared to the spectrum of the starting clay, which may correspond to the lesser amount of Cu that was exchanged.

In the lower region (1800-400 cm^{-1}), the only changes observed were those of H_2O bending bands and organics bands. Both H_2O bending bands have been shifted downwards even more than in the Series a, moving from around 1690 and 1640 cm^{-1}, down to 1670 and 1630 cm^{-1}, respectively.

The 3630 cm^{-1} band stays unchanged, but the other bands in the 3500-3000 cm^{-1} region have been shifted. The (cation-OH) H-bonded band has shifted by 30 to 40 cm^{-1} upwards, which was about twice as much as seen in the Series a spectra. Opposite to what was seen in the Series a spectra, (OH-OH) H bonded and (H_2O) bend overtone bands have been shifted to 3416-3408 cm^{-1} and 3310-3300 cm^{-1}, respectively. (Cu^{2+}-OH, Al^{3+}-OH) moves only slightly, 4 to 5 cm^{-1}, downwards.

Fig. 3b shows the relationship between the intensities of bands at 3630 and 3500 cm^{-1}, relative to the starting Cu solution concentration. The same polynomial trendline is fitted to the graph even though the curve is 'flatter' in Series b than in Series a. This might correspond, perhaps, to a lower amount of Cu exchange in Series b samples than in Series a samples.

Cu-exchanged Miles montmorillonite

Apart from the differences in the composition which were discussed previously, Miles montmorillonite follows similar changes, in terms of the relationship between the intensities of two bands in the OH- region, when Cu-exchanged (Fig. 4). However, when the (cation-OH) H-bonded band over (Al_2OH) stretching band ratio is plotted against the Cu concentration of the starting solution, in Fig. 5a, a trendline does not provide as good fit as for Cheto montmorillonite samples.

Bands at 3635 cm^{-1}, due to the Al_2OH stretching mode, and 3480 cm^{-1}, due to the (cation-OH) H-bonded vibration, are shifted upwards and brought closer together. Other bands, at 3400, 3290 and 3186 cm^{-1}, remain unchanged with the Cu loading. Furthermore new bands emerge in this region, around 3120 and 3020 cm^{-1} for all Series a samples, which are probably due to the Cu^{2+}-OH vibration.

The H_2O bending vibrations at 1652 and 1634 cm^{-1} are both shifted to higher wavenumbers, 1670 and 1637 cm^{-1}, respectively. In addition, Series a Miles montmorillonite also contains a band around 1400 cm^{-1}, assigned to ammonia molecules being trapped within the structure or absorbed on the surface of the clay.

All changes in Series b are concentrated in the 3650-3000 cm^{-1} region, as the remaining part of the spectra is almost identical to the starting Miles montmorillonite. Similar to Series a, the Al_2OH stretching mode and the (cation-OH) H-bonded mode are both shifted to higher wavenumbers, around 3638 and 3530-3500 cm^{-1}, respectively. The same is observed for the (OH-OH) H bond, which, in Series b, is around 3418-3408 cm^{-1}, while bands at 3290 and 3186 cm^{-1} remain unchanged.

The 'relationship curve' in Fig. 5b is quite 'flat', which, in combination with practically unchanged infrared spectra, suggests that Series b Cu-exchanged Miles montmorillonite has undergone only a small amount of cation exchange.

Infrared emission spectroscopy

Cheto vs Miles montmorillonite

In IES, both, Cheto and Miles montmorillonite, give similar spectra (Fig. 6). Major changes are observed for the H_2O bending mode around 1625 (Cheto) and 1630 (Miles) cm^{-1}, together with Si-O-Si stretching modes around 1040 (Cheto) and 1050 (Miles) cm^{-1}. Other bands are observed around 920 cm^{-1}, due to (Al_2OH) deformation, and 850 cm^{-1}, due to (MgAlOH) deformation. H_2O OH-stretching modes at 3500 and 1635 cm^{-1} are very weak in both clays as most of the H_2O has evaporated before the samples reached 150°C.

Consistent with the theory, presented in the introductory section, most of absorbed H_2O has been removed before two samples reached the starting experimental 150°C temperature. The next dehydration stage occurred between 150 and 300°C where the H_2O of the cation hydration shell is evolved. The last dehydration occurred between 300 and 600°C, due to more than one hydration shell around more polarisable cations, after which no H_2O remains in the montmorillonite structure. Si-O-Si bands, together with the quartz bands in the Miles clay, remain unchanged with the heating.

Cu-exchanged montmorillonites

It is more useful to compare the different preparation methods of Cu-exchanged montmorillonite than to assess them separately since there are no significant differences between the two montmorillonite types.

In Series a Cu-exchanged montmorillonites, the same bands from the starting montmorillonites have been preserved, but two new bands, unique to this group, have emerged around 3270 and 1425 cm^{-1}. These both bands have been attributed to ammonia molecules, with a very small proportion of the 3270 cm^{-1} band being contributed by hydroxyl groups. The assignment of bands was made easy after the spectra were compared to TGA data [8], which showed the evolvement of ammonia gas by Series a samples and that it ceased around 500°C, identical to the IES results. The presence of ammonia molecules within the structure of montmorillonites therefore proves that cation exchange has taken place to some degree.

Series b Cu-exchanged montmorillonites have identical spectrum to starting montmorillonite type, in terms of both, band position and band assignment. Furthermore it is interesting to note that Cu-exchanged montmorillonites using lower starting Cu-solution concentrations give much better resolution spectrum than if higher Cu concentrations were used and this is the case for both monmorillonite types.

CONCLUSION

Mid Infrared Spectroscopy (Mid-IR) and Infrared Emission Spectroscopy (IES) were employed to characterise Cu-exchanged Cheto and Miles montmorillonites. All Cu-

exchanged montmorillonites experienced a shift in most of non-lattice bands. In addition, a relationship between the ratio of bands at 3630 and 3500 cm^{-1} and the Cu-concentration of the starting solutions was observed and used to compare the degree of cation exchange between the two preparation methods. Infrared emission spectroscopy was used to characterise the thermal behaviour of Na^{+}, Ca^{2+} and Cu^{2+}-exchanged montmorillonites. Two distinct dehydration stages were observed associated with interlayer water loosly bound and more strongly bound to the interlayer cations as well as the evolution of ammonia from the Cu-exchanged montmorillonite samples prepared by the 'basic' method.

ACKNOWLEDGMENTS

We would like to thank Dr Zhe Ding for supplying the samples and all her help along the way. Other people that also must be mentioned are Wayde Martens and Llew Rintoul as they have all contributed to this project in some way.

REFERENCES

[1] C. E. Weaver, L. D. Pollard, The Chemistry of Clay Minerals, Elsevier Scientific Publishing Company, Amsterdam, 1973.
[2] R. W. Grimshaw, The Chemistry and Physics of Clays and Allied Ceramic Materials, 4th ed., Ernest Benn Limited, London, 1971.
[3] W. E. Worrall, Clays and Ceramic Raw Materials, 2nd ed., Elsevier Scientific Publishing Company, London, 1986.
[4] W. A. Deer, R. A. Howie, J. Zussman, An introduction to the Rock-Forming Minerals, 2nd ed., Addison Wesley Longman Ltd., Harlow, 1996.
[5] L. Montaland, 1911.
[6] E. Houdry, W. F. Burt, A. E. Pew Jr., W. A. Peters Jr., Nat. Pet. News 37 (1938) R570.
[7] J. T. Kloprogge, J. Porous Materials 5 (1998) 5.
[8] Z. Ding, J. T. Kloprogge, R. L. Frost, G. Q. Lu, H. Y. Zhu, J. Por. Mater. 8 (2001) 273.
[9] M. Auboiroux, F. Melou, F. Bergaya, J. C. Touray, Clays Clay Miner. 46 (1998) 546.
[10] J. Comets, L. Kevan, J. Phys. Chem. 97 (1993) 466.
[11] T. Matsuda, K. Yogo, C. Pantawong, E. Kikuchi, Appl. Catal. A 126 (1995) 177.
[12] A. C. D. Newman, Chemistry of clay and clay minerals, Vol. 6, Longman Scientific & Technical, Harlow, UK, 1987.
[13] R. van Bladel, H. Halen, P. Cloos, Clay Miner. 28 (1993) 33.
[14] H. P. He, J. G. Guo, X. D. Xie, J. L. Peng, Env. Int. 26 (2001) 347.
[15] M. Stadler, P. W. Schindler, Clays Clay Miner. (1993) 148.
[16] C. Bertin, A. C. M. Bourg, Water Research 29 (1995).
[17] J. N. Nwankwo, C. G. Elinder, Bulletin of Environmental Contamination and Toxicology 22 (1979) 625.
[18] C. N. Hewitt, M. B. Rashed, Water Research 26 (1992) 311.
[19] M. F. Brigatti, F. Corradini, G. C. Franchini, S. Mazzoni, L. Medici, L. Poppi, Appl. Clay Sci. 9 (1995) 383.
[20] M. Auboiroux, P. Bailif, J. C. Touray, F. Bergaya, Appl. Clay Sci. 11 (1996) 117.
[21] C. Craciun, Thermochim. Acta 117 (1987) 25.
[22] L. Heller-Kallai, C. Mosser, Clays Clay Miner. 43 (1995) 738.
[23] J. Madejova, B. Arvaiova, P. Komadel, Spectrochim. Acta, A 55A (1999) 2467.
[24] C. Mosser, L. J. Michot, F. Villieras, M. Romeo, Clays Clay Miner. 45 (1997) 789.
[25] J. T. Kloprogge, R. Evans, L. Hickey, R. L. Frost, Appl. Clay Sci. 20 (2002) 157.
[26] A. M. Vassallo, P. A. Cole-Clarke, L. S. K. Pang, A. Palmisane, J. Applied Spectroscopy 46 (1992) 73.
[27] R. L. Frost, B. M. Collins, K. Finnie, A. J. Vassallo, Proc. 10th Int. Clay Conf. (1995) 219.

[28] R. L. Frost, A. M. Vassallo, Clays Clay Miner. 44 (1996) 635.
[29] V. Farmer, The Infrared Spectra of Minerals, Mineralogical Society, England, 1974.
[30] J. L. Bishop, C. M. Pieters, J. O. Edwards, Clays Clay Miner. 42 (1994) 702.

Table 1 Overview of the main Mid-IR bands (cm^{-1}) of montmorillonite before and after Cu-exchange.

Cheto	Miles	Series a		Series b		Assignment
		Cheto	Miles	Cheto	Miles	
3630	3635	3632	3637	3630	3638	Al-OH-stretch
3400-3470	3400-3480	3390-3480	3400-3490	3410-3505	3410-3530	Water OH-stretch
		3170		3172		Cu^{2+}-OH stretch
1691		1680		1670		Water OH-bend
1635	1634		1637		1636	Water OH-bend
		1400				ammonia
1090	1100	1086	1105	1088	1108	Si-O-Si stretch
1040	1050	1037	1050	1035	1050	Si-O-Si stretch
910	917	909	915	909	915	Al_2-OH deformation
840	846	838	846	839	845	AlMg-OH deformation
520	523	517	522	517	522	Si-O-Al bend
467	468	465	467	465	467	Si-O-Si bend

Figure captions

Fig. 1 a) The infrared OH-stretching region (3700-2800 cm^{-1}) and b) the lower wavenumber region (400-1800 cm^{-1})of Cheto montmorillonite.

Fig. 2 Infrared spectra **i)** (3700-2800cm^{-1}) and **ii)** (1800-400 cm^{-1}) of **a)** Cheto montmorillonite, and Series *a* Cu-exchanged Cheto montmorillonite: **b)** Cha3, **c)** Cha1 and **d)** Cha2.

Fig. 3 (Al_2OH) band / (OH-OH) H bonded band ratio plotted against copper loading solution concentration for Cheto montmorillonite a) Series a and b) Series b. (the dashed curve is a fitted polynomial trendline).

Fig. 4 Infrared spectra **i)** (3700-2800cm^{-1}) and **ii)** (1800-400 cm^{-1}) of **a)** Miles montmorillonite, and Series *a* Cu-exchanged Miles montmorillonite: **b)** Mia3, **c)** Mia1 and **d)** Mia2.

Fig. 5 (Al_2OH) band / (OH-OH) H bonded band ratio plotted against copper loading solution concentration for Miles montmorillonite **a)** Series a and **b)** Series b. (the dashed curve is a fitted polynomial trendline).

Fig. 6 IES spectra of Cha1 from T1 = 150°C to T2 = 800°C with readings taken at 50°C steps. (a = (MgAlOH) deformation, b = (Al2OH) deformation).

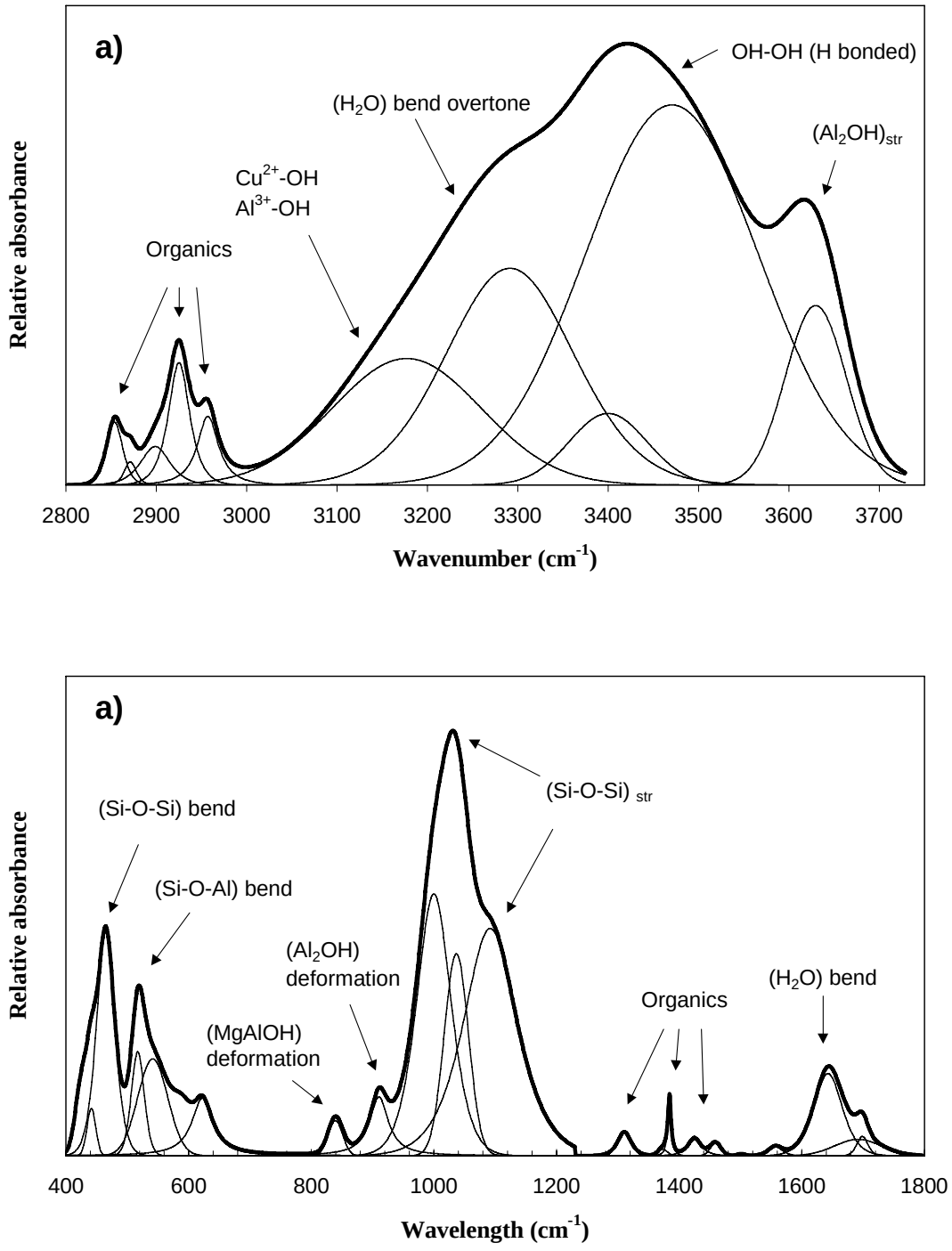
a)
OH-OH (H bonded)
(H2O) bend overtone
(Al2OH)str
Cu2+-OH
Al3+-OH
Organics
Relative absorbance
2800
2900
3000
3100
3200
3300
3400
3500
3600
3700
Wavenumber (cm-1)
a)
(Si-O-Si) bend
(Si-O-Si) str
(Si-O-Al) bend
(Al2OH)
deformation
(MgAlOH)
deformation
Organics
(H2O) bend
Relative absorbance
400
600
800
1000
1200
1400
1600
1800
Wavelength (cm-1)

Figure 1

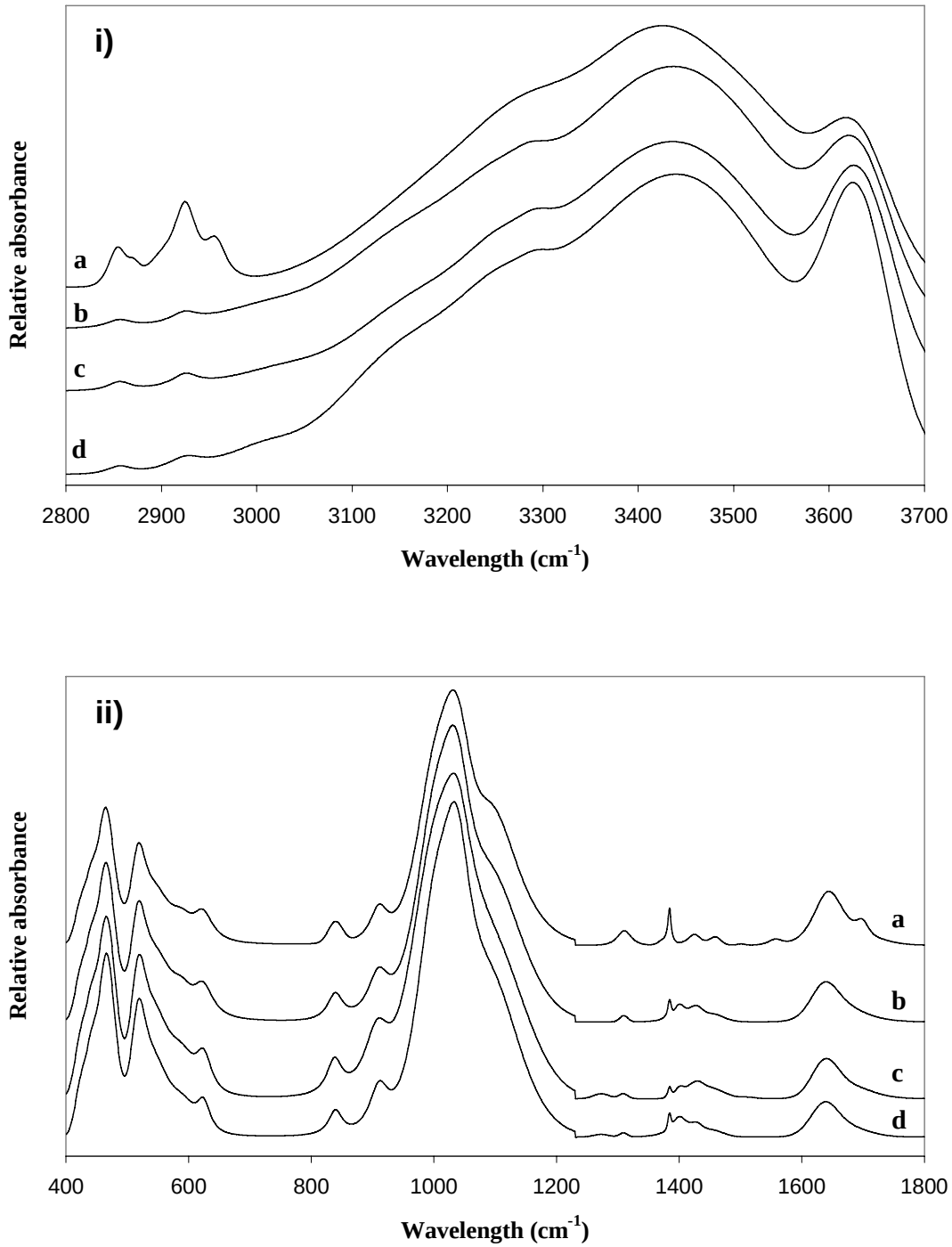
i)
Relative absorbance
a
b
c
d
2800
2900
3000
3100
3200
3300
3400
3500
3600
3700
Wavelength (cm-1)
ii)
Relative absorbance
a
b
c
d
400
600
800
1000
1200
1400
1600
1800
Wavelength (cm-1)

Figure 2

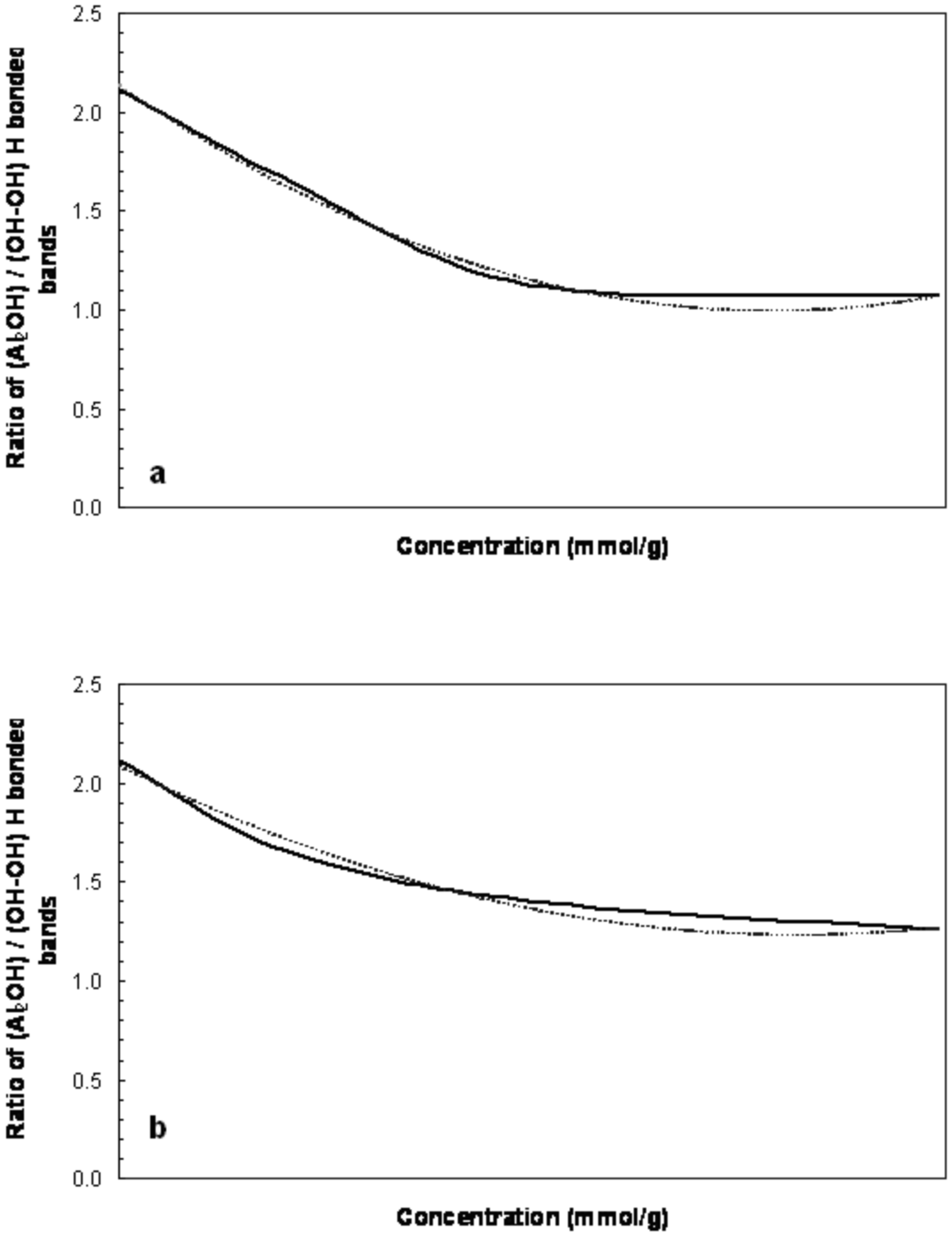
Ratio of (AlOH) / (OH-OH) H bonded bands
2.5
2.0
1.5
1.0
0.5
0.0
a
Concentration (mmol/g)
Ratio of (AlOH) / (OH-OH) H bonded bands
2.5
2.0
1.5
1.0
0.5
0.0
b
Concentration (mmol/g)

Figure 3

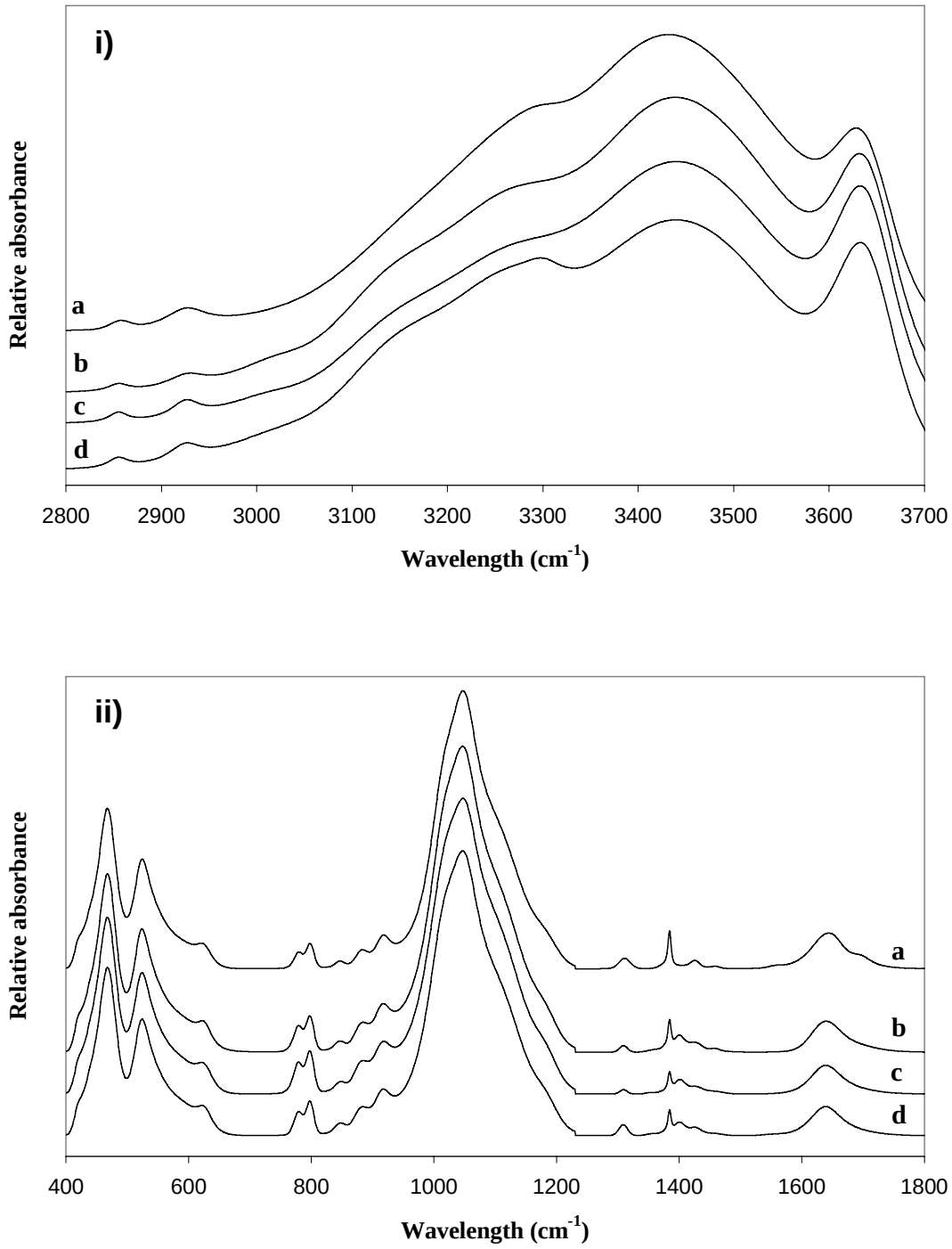
i)
Relative absorbance
a
b
c
d
2800
2900
3000
3100
3200
3300
3400
3500
3600
3700
Wavelength (cm-1)
ii)
Relative absorbance
a
b
c
d
400
600
800
1000
1200
1400
1600
1800
Wavelength (cm-1)

Figure 4

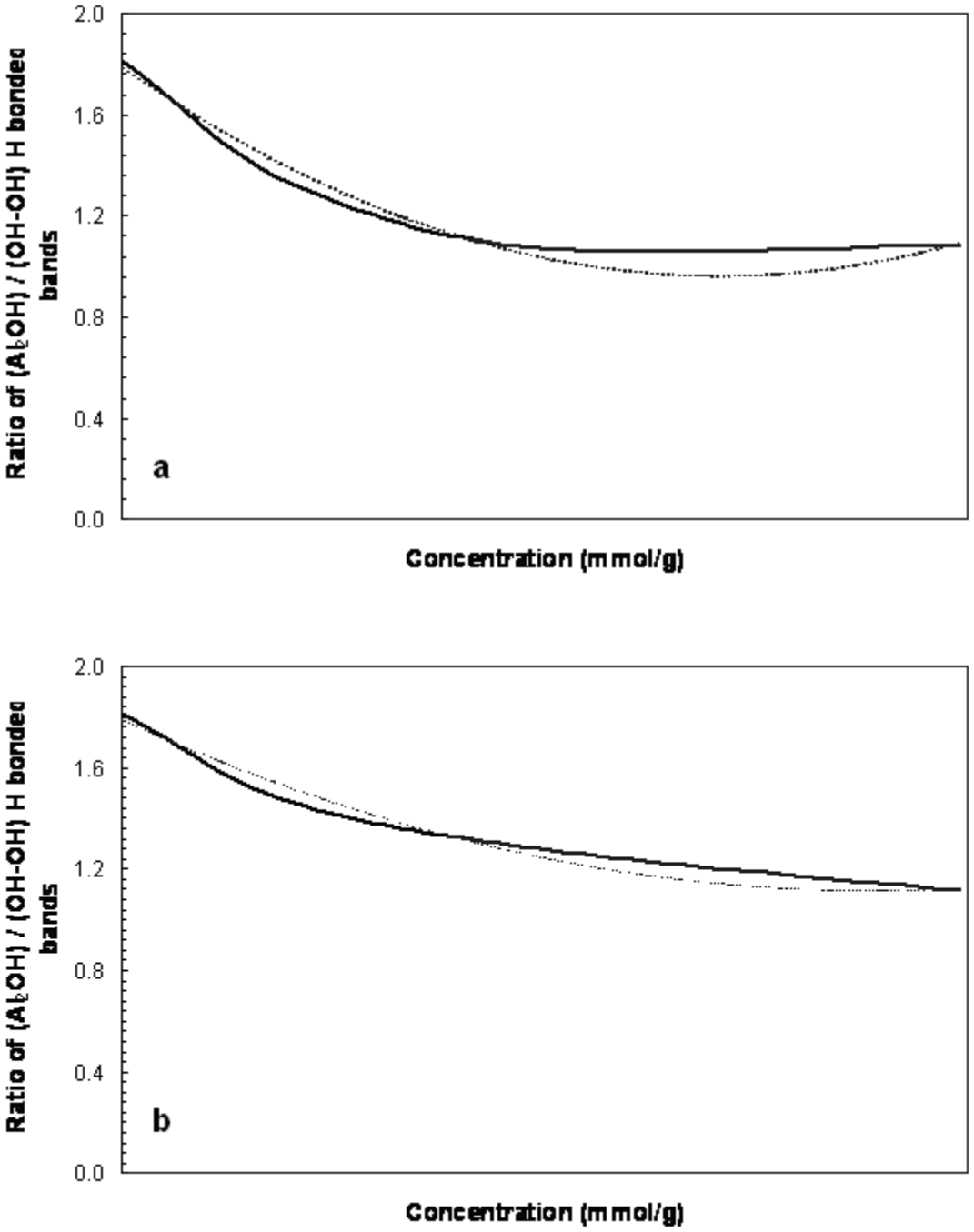
Ratio of (AlOH) / (OH-OH) H bonded bands
2.0
1.6
1.2
0.8
0.4
0.0
a
Concentration (mmol/g)
Ratio of (AlOH) / (OH-OH) H bonded bands
2.0
1.6
1.2
0.8
0.4
0.0
b
Concentration (mmol/g)

Figure 5

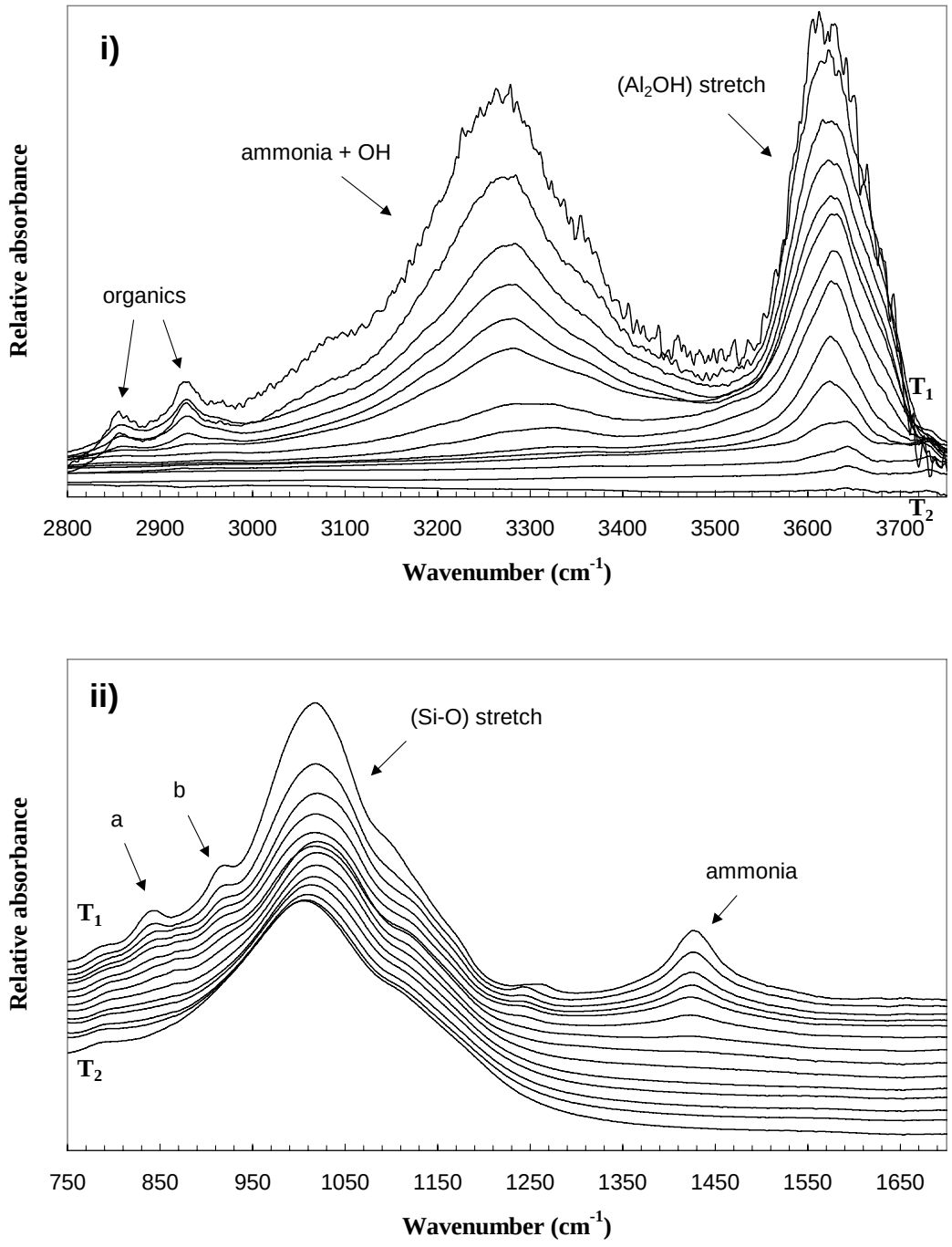
i)
(Al2OH) stretch
ammonia + OH
organics
Relative absorbance
T1
T2
2800
2900
3000
3100
3200
3300
3400
3500
3600
3700
Wavenumber (cm-1)
ii)
(Si-O) stretch
b
a
ammonia
T1
T2
Relative absorbance
750
850
950
1050
1150
1250
1350
1450
1550
1650
Wavenumber (cm-1)

Figure 6